

# Superconductivity and magnetism in noncentrosymmetric LaPtGe<sub>3</sub> and CePtGe<sub>3</sub>

Manuel Feig,<sup>1,2</sup> Michael Nicklas,<sup>2</sup> Matej Bobnar,<sup>2</sup> Walter Schnelle,<sup>2</sup> Ulrich Schwarz,<sup>2</sup> Andreas Leithe-Jasper,<sup>2</sup> Christoph Hennig,<sup>3,4</sup> and Roman Gumeniuk<sup>1,2,\*</sup>

<sup>1</sup>Institut für Experimentelle Physik, TU Bergakademie Freiberg, Leipziger Straße 23, 09596 Freiberg, Germany

<sup>2</sup>Max-Planck-Institut für Chemische Physik fester Stoffe, Nöthnitzer Straße 40, 01187 Dresden, Germany

<sup>3</sup>Helmholtz-Zentrum Dresden-Rossendorf, Institute of Resource Ecology, Bautzner Landstraße 400, 01328 Dresden, Germany

<sup>4</sup>The Rossendorf Beamline at ESRF, CS 40220, 38043 Grenoble Cedex 9, France



(Received 10 August 2018; revised manuscript received 24 September 2018; published 26 November 2018)

LaPtGe<sub>3</sub> and CePtGe<sub>3</sub> crystallize with a noncentrosymmetric body-centered tetragonal (space group *I4mm*) BaNiSn<sub>3</sub>-type of structure. LaPtGe<sub>3</sub> is a weakly coupled BCS-like *s*-wave type-I superconductor with  $T_c = 0.55$  K,  $B_c \simeq 14$  mT, and Ginzburg-Landau parameter  $\kappa_{GL} = 0.021 < 1/\sqrt{2}$ . CePtGe<sub>3</sub> is a nonsuperconducting ( $T_{nsc} = 0.35$  K) metal with an effective magnetic moment  $\mu_{eff} = 2.46\mu_B$ . The Ce moments show two antiferromagnetic ordering transitions at  $T_{N1} \approx 3.7$  K and  $T_{N2} \approx 2.7$  K and a ground-state multiplet  $J = 5/2$  splitting into three doublets (energy splittings from the ground state  $\Delta_1 = 46$  K and  $\Delta_2 = 137$  K). The moderately enhanced Sommerfeld coefficient  $\gamma_0$  and the observation of almost the full critical magnetic entropy at  $T_{N1}$  suggest that magnetic Ruderman-Kittel-Kasuya-Yosida-type interactions are dominant in CePtGe<sub>3</sub>, leading to a magnetically ordered ground state.

DOI: 10.1103/PhysRevB.98.184516

## I. INTRODUCTION

Superconductors (SCs) revealing unconventional mechanisms which do not obey the BCS theory and its strong electron-phonon coupling extensions attract special attention in modern solid-state science. Very frequently such effects can be observed in compounds crystallizing in crystal structures without a center of inversion. Noncentrosymmetric spatial symmetry can give rise to a Rashba-type antisymmetric spin-orbit coupling and thus the mixing of spin-singlet and spin-triplet Cooper-pairing channels. This may result in a multicomponent order parameter and enhanced upper critical field  $B_{c2}$ , which is then much higher than the Pauli limit [1]. The most prominent examples of noncentrosymmetric SCs with unusual superconducting mechanisms are LaNiC<sub>2</sub>, Mo<sub>3</sub>Al<sub>2</sub>C, and Li<sub>2</sub>Pt<sub>3</sub>B. As shown in [2,3] the time-reversal symmetry-breaking triplet state in LaNiC<sub>2</sub> can exist only with weak antisymmetric spin-orbit coupling. The spin-triplet Cooper pairing in Mo<sub>3</sub>Al<sub>2</sub>C is assumed in [4,5] to be mainly due to the possibility of a nodal gap. However, later studies [6,7] reported a fully opened gap with the previous evidence for nodal SC being ascribed to an impurity phase. The superconductivity in Li<sub>2</sub>Pt<sub>3</sub>B is based on a mixture of singlet and triplet components, rather than a pure spin-triplet pairing state [8,9].

The discovery of these compounds in the past decade gave strong impetus to the investigation of ternary silicides and germanides with 1:1:3 stoichiometry. Typical compounds consist of alkaline-earth (*A*), rare-earth (*R*), and transition (*T*) *d* metals of IX–XI subgroups. Crystallizing with the tetragonal body-centered noncentrosymmetric BaNiSn<sub>3</sub>-type

of structure (space group *I4mm*) [10] {*A*, *R*}*T*{Si, Ge}<sub>3</sub> (*R* = nonmagnetic rare earth) seemed to fulfill the above-mentioned conditions for unconventional SCs. However, further investigations indicated a simple *s*-wave BCS-like superconductivity with transition temperatures  $T_c < 4$  K and rather low critical magnetic fields  $B_{c2} < 500$  mT for SrNiSi<sub>3</sub> [11], CaIrSi<sub>3</sub> [12–15], APdSi<sub>3</sub> (*A* = Sr, Ba [11]), MPtSi<sub>3</sub> (*M* = Ca [16,17], Sr [11], Ba [18–20], La [21,22]), SrAuSi<sub>3</sub> [23–25], SrPdGe<sub>3</sub>, and SrPtGe<sub>3</sub> [11,20]. Moreover, combined muon spin rotation and transport property studies unexpectedly showed such ternary complex compounds as LaRhSi<sub>3</sub> ( $T_c = 2.16$  K;  $B_c = 17.2$  mT) [26], LaIrSi<sub>3</sub> ( $T_c = 0.72$  K;  $B_c = 6$  mT) [27,28], and LaPdSi<sub>3</sub> ( $T_c = 2.65$  K;  $B_c = 18.3$  mT) [21] to be simple type-I SCs. Interestingly, no superconductivity is observed for the La{Rh, Ir, Pd}Ge<sub>3</sub> germanides down to 0.35 K [29,30].

The combination of noncentrosymmetric crystal structure with strong *f*-electron correlations, as in CePt<sub>3</sub>Si, leads to such interesting phenomena as the coexistence of magnetic ordering, the heavy-fermion effect, and superconductivity [31,32]. Such cases are of special interest because the Cooper pairs are then believed to consist of electrons with enhanced masses. Analogous to CePt<sub>3</sub>Si, such a behavior is induced by applying high pressure in CeTSi<sub>3</sub> (*T* = Rh [33–35], Ir [36–38]) and CeTGe<sub>3</sub> (*T* = Co [39,40], Rh [41], Ir [42]), which crystallize with a BaNiSn<sub>3</sub>-type of structure. In *R*-Pt-Ge systems only one isostructural, EuPtGe<sub>3</sub>, germanide is reported to exist [43]. It is an antiferromagnet with  $T_N = 11$  K and two antiferromagnetically coupled Eu<sup>2+</sup> sublattices.

Investigating *R*-Pt-Ge systems, we succeeded in the preparation of *R*<sub>3</sub>Pt<sub>4</sub>Ge<sub>13</sub> phases under high pressure (where *R* = Y, Pr, Sm, Gd, Tb, Tm, Yb) [44–46] with crystal structures derived from the primitive cubic Yb<sub>3</sub>Rh<sub>4</sub>Sn<sub>13</sub> of the Remeika type [47]. Therefore, the question of whether isostructural compounds with light *R* atoms (La-Sm) could be obtained

\*roman.gumeniuk@physik.tu-freiberg.de

arose. However, applying high-pressure synthesis, we observed the formation of germanides with the  $\{\text{La, Ce}\}\text{PtGe}_3$  composition crystallizing with a tetragonal noncentrosymmetric  $\text{BaNiSn}_3$ -type of structure instead of the 3:4:13 target compounds. Further syntheses of the samples with 1:1:3 compositions revealed that  $\text{LaPtGe}_3$  can be synthesized by the annealing of the arc-melted specimen, while  $\text{CePtGe}_3$  can be obtained only by applying a high-pressure technique (i.e., 8 GPa and 850 °C). The studies of magnetic and transport properties revealed  $\text{LaPtGe}_3$  to be a type-I BCS-like superconductor with low  $T_c$  and  $\text{CePtGe}_3$  to be a  $\text{Ce}^{3+}$  stable-valent antiferromagnet with a complex magnetic structure displaying no SC down to  $T_{\text{nsc}} = 0.35$  K.

## II. EXPERIMENT

$\text{LaPtGe}_3$  and  $\text{CePtGe}_3$  samples were synthesized from lanthanum and cerium ingots (Ames, 99.9 wt %), platinum foil (Chempur, 99.95 wt %), and crystalline germanium (Chempur, 99.9999 wt %). The starting materials were arc melted (mass loss of <0.5%), sealed in tantalum tubes enclosed in evacuated silica ampoules, heat treated at 700 °C or 850 °C for 240 h, and quenched in water. The samples were handled in argon-filled glove boxes [ $p(\text{O}_2/\text{H}_2\text{O}) < 1$  ppm]. After such synthesis the  $\text{LaPtGe}_3$  sample was found to be single phase (see text below). Since the  $\text{CePtGe}_3$  sample was multiphasic after the treatments described above, it was used as a precursor for high-pressure synthesis, which was performed in a multianvil press at 8 GPa and 850°C. The force redistribution in the press was realized by a Walker module and  $\text{MgO}$  octahedra with edge lengths of 18 mm [48]. Boron nitride crucibles were used as a sample container. The typical annealing time was 2 h, followed by quenching to room temperature by switching off the heating before decompression. The ingot could be easily recovered from the crucible and proved to be stable in air.

All samples were characterized by powder x-ray diffraction (XRD) on a Guinier camera G670, with  $\text{Cu } K\alpha_1$  radiation. High-resolution (HR) powder XRD data for structure refinement were collected at room temperature at the BM20 beamline of the European Synchrotron Radiation Facility (ESRF, Grenoble;  $\lambda = 0.45923 \text{ \AA}$ ,  $2\theta_{\text{max}} = 45^\circ$ ) on powder enclosed in a quartz capillary with an outer diameter of 0.3 mm. The images acquired on a Pilatus3 X 2M detector [49] were integrated with the BUBBLE software [50], which is based on the PYFAI library [51]. The phase analysis was performed using the WINXPOW program package [52]. The lattice parameters and crystal structures were refined by least-squares fitting (program package WINCSd [53]).

The magnetization was measured with a superconducting quantum interference device magnetometer (MPMS XL-7, Quantum Design). The electrical resistivity and the heat capacity were measured down to 0.35 K (PPMS9, Quantum Design) using an ac resistivity bridge (LR-700, Linear Research) and the heat capacity option of the PPMS9, respectively. Electrical contacts were made with silver-filled epoxy.

The electronic structure of  $\text{LaPtGe}_3$  was calculated within the local-density approximation of the density-functional theory (DFT) using the full-potential FPLO code (version 9.01-35) [54] with the basis set of local orbitals. In the scalar relativistic

TABLE I. Crystallographic data and interatomic distances  $d$  for  $\text{LaPtGe}_3$  and  $\text{CePtGe}_3$  (structure type  $\text{BaNiSn}_3$ , space group  $I4mm$ ,  $Z = 2$ ).

	Compound	
	$\text{LaPtGe}_3$	$\text{CePtGe}_3$
$a (\text{\AA})$	4.5064(2)	4.4922(4)
$c (\text{\AA})$	9.8239(4)	9.807(1)
$V (\text{\AA}^3)$	199.50(3)	197.90(5)
$\rho (\text{g cm}^{-3})$	9.19(1)	9.28(1)
Wavelength $\lambda (\text{\AA})$	0.45923	1.54056
$R_{\text{l}}/R_{\text{p}}$	0.027/0.073	0.045/0.104
$R$ in $2a (0, 0, z), z$	0.0001(1)	0.0001(1)
$B_{\text{iso}}$	1.11(3)	1.3(1)
$d(R-4\text{Ge}2) (\text{\AA})$	3.262(2)	3.234(7)
$d(R-4\text{Ge}1) (\text{\AA})$	3.3261(8)	3.312(4)
$d(R-4\text{Ge}2) (\text{\AA})$	3.405(2)	3.418(7)
$d(R-1\text{Pt}) (\text{\AA})$	3.412(2)	3.406(6)
$d(R-4\text{Pt}) (\text{\AA})$	3.5217(7)	3.512(3)
$d(R-1\text{Ge}1) (\text{\AA})$	3.958(3)	3.97(1)
Pt in $2a (0, 0, z), z$	0.3474(2)	0.3474(7)
$B_{\text{iso}}$	1.08(2)	1.2(1)
$d(\text{Pt}-1\text{Ge}1) (\text{\AA})$	2.453(3)	2.43(1)
$d(\text{Pt}-4\text{Ge}2) (\text{\AA})$	2.487(1)	2.492(5)
Ge1 in $2a (0, 0, z), z$	0.5971(3)	0.595(1)
$B_{\text{iso}}$	1.08(4)	1.2(1)
$d(\text{Ge}1-4\text{Ge}2) (\text{\AA})$	2.656(2)	2.642(8)
Ge2 in $4b (0, 1/2, z), z$	0.2401(3)	0.237(1)
$B_{\text{iso}}$	1.18(4)	1.3(1)
$d(\text{Ge}2-4\text{Ge}2) (\text{\AA})$	3.1865(1)	3.1765(2)

calculation the exchange-correlation potential by Perdew and Wang [55] was used. The  $k$  mesh included 27 000 points in the full Brillouin zone.

## III. RESULTS AND DISCUSSION

### A. Crystal structures of $\{\text{La, Ce}\}\text{PtGe}_3$

All 174 peaks in the HR synchrotron XRD pattern of  $\text{LaPtGe}_3$  sample were indexed in a tetragonal lattice with the unit cell parameters given in Table I. The analysis of extinction conditions indicated eight possible body-centered space groups (SGs) of the diffraction symbol  $I \bar{4} \bar{3} \bar{m}$ . In the beginning we performed the refinement of the crystal structure assuming the SG  $I4/mmm$  (highest possible symmetry) and thus the structural model of the  $\text{ThCr}_2\text{Si}_2$  type [57]. However, it resulted in the wrong  $\text{LaPt}_{2.4}\text{Ge}_{1.6}$  composition and unacceptably high reliability factors  $R_{\text{l}} = 0.100$  and  $R_{\text{p}} = 0.201$ . The  $\text{ThCr}_2\text{Si}_2$  model fails completely to describe numerous peaks in the HR XRD pattern of  $\text{LaPtGe}_3$  [Fig. 1(b)]. Therefore, the structural model of the noncentrosymmetric (SG  $I4mm$ )  $\text{BaNiSn}_3$  type [10] was used. The final parameters of this refinement are collected in Table I, and the experimentally measured, theoretically calculated, and differential profiles are depicted in Fig. 1(a). The crystallographic parameters together with the low values of  $R$  factors confirm the noncentrosymmetric nature of the structure of  $\text{LaPtGe}_3$ .

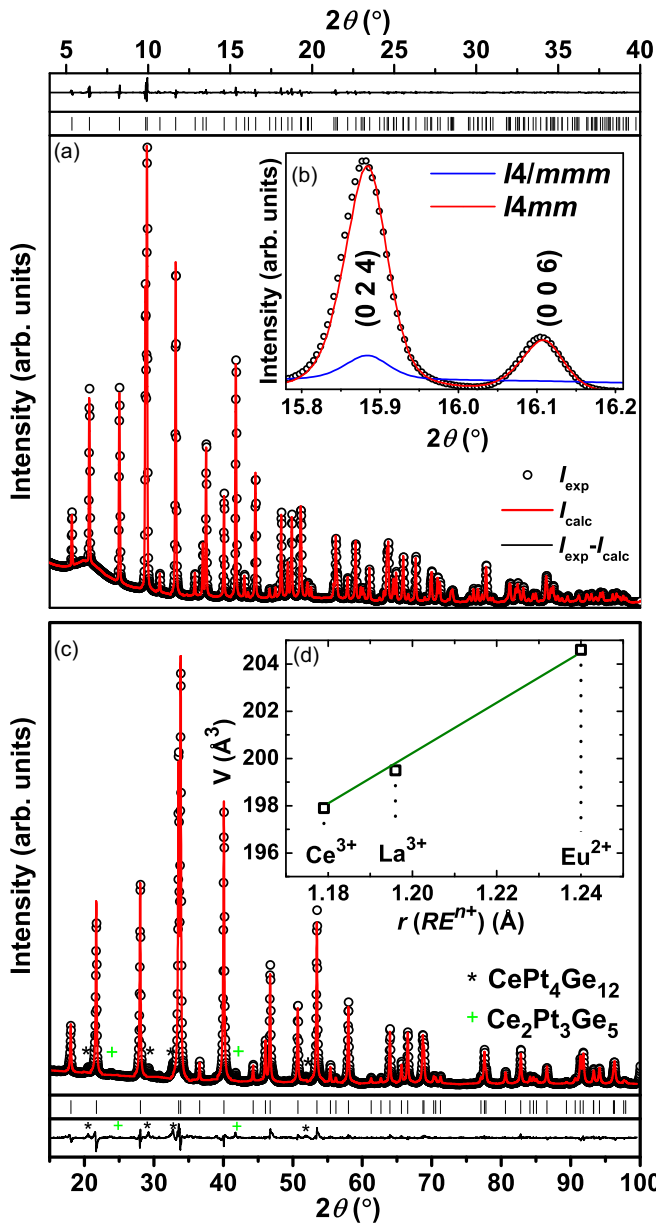


FIG. 1. Experimental, calculated, and difference XRD patterns together with the peak positions for (a) LaPtGe<sub>3</sub> and (c) CePtGe<sub>3</sub>. Background-to-intensity ratios are 11 and 22, respectively. (b) The (0 2 4) and (0 0 6) reflections assuming centro- and noncentrosymmetric structural models. (d) Dependence of unit cell volumes of RPtGe<sub>3</sub> ( $R = \text{La}, \text{Ce}, \text{Eu}$  [43]) versus ionic radii of  $R^{n+}$  ions [56].

The phase analysis of the powder XRD pattern for a CePtGe<sub>3</sub> sample annealed at 700 °C for 6 days revealed it to be inhomogeneous and to consist of five phases: elemental germanium, CePtGe<sub>2</sub> [59], Ce<sub>3</sub>Pt<sub>4</sub>Ge<sub>6</sub> [60], CePt<sub>2</sub>Ge<sub>2</sub> [61], and CePt<sub>4</sub>Ge<sub>12</sub> [62]. After high-pressure treatment, the majority noncentrosymmetric CePtGe<sub>3</sub> with the BaNiSn<sub>3</sub> type of structure phase [10] together with a small admixture of CePt<sub>4</sub>Ge<sub>12</sub> and Ce<sub>2</sub>Pt<sub>3</sub>Ge<sub>5</sub> [63] was identified [Fig. 1(c)]. Since the impurities do not contribute to the x-ray intensities of the main phase, the peaks corresponding to these impurity phases were excluded from the further Rietveld refinement, which converged to the parameters presented in Table I.

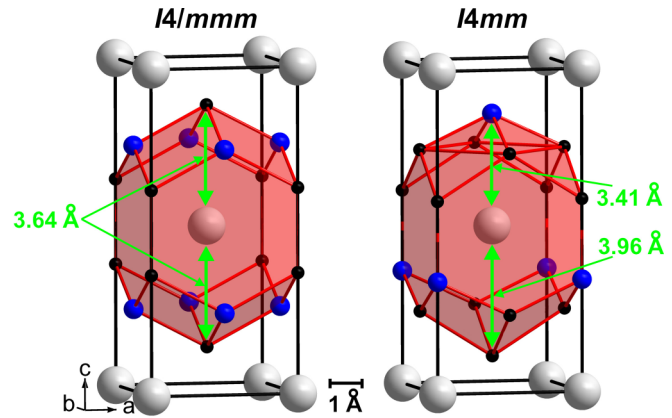


FIG. 2. Crystal structures of LaPt<sub>2</sub>Ge<sub>2</sub> (SG I4/mmm, ThCr<sub>2</sub>Si<sub>2</sub> type; left) [58] and LaPtGe<sub>3</sub> (I4mm type; right). La atoms are shown in light gray, Pt atoms are in blue, and Ge atoms are shown as black balls. The distortions in the latter structure are visible in the changes in distances between the central La atoms and the tops of the 18-vertex polyhedron.

The refined interatomic distances in the crystal structures of LaPtGe<sub>3</sub> and CePtGe<sub>3</sub> correlate well with the sum of atomic radii of the elements ( $r_{\text{La}} = 1.88 \text{ \AA}$ ;  $r_{\text{Ce}} = 1.82 \text{ \AA}$ ;  $r_{\text{Pt}} = 1.38 \text{ \AA}$ ;  $r_{\text{Ge}} = 1.23 \text{ \AA}$ ) [64].  $R$ -Ge,  $R$ -Pt, and Ge-Ge contacts are slightly larger than the corresponding sums, while Pt-Ge distances are shorter by 6%–7%. The dependence of the unit cell volumes of known RPtGe<sub>3</sub> ( $R = \text{La}, \text{Ce}, \text{Eu}$  [43]) germanides versus ionic radii of  $R^{n+}$  ions [56] is plotted in Fig. 1(d). The observed linear dependence suggests a stable 3+ oxidation state for Ce (and La) in the studied compounds.

The close structural relationship of the ThCr<sub>2</sub>Si<sub>2</sub> [57] and BaNiSn<sub>3</sub> [10] types on the basis of a group-subgroup scheme was discussed in [65]. As one can see from Fig. 2, the *translationsgleiche* symmetry reduction of index 2 (i.e., transition from SG I4/mmm to I4mm) results from different site occupancies and slight distortions (shown for the example of the shift of two vertices in the coordination polyhedron of La atoms).

## B. LaPtGe<sub>3</sub>

The magnetic susceptibility  $\chi(T)$  for LaPtGe<sub>3</sub> is depicted in Fig. 3(a). It is diamagnetic in the whole measured temperature range with  $\chi_0 = -97 \times 10^{-6} \text{ emu mol}^{-1}$ . An upturn below 100 K is due to a minor paramagnetic impurity contribution ( $0.085 \mu_B$ , equivalent to 0.24% of magnetic  $S = 1/2$  species). The measured  $\chi(T)$  reveals no indications of any phase transition in the temperature range 1.8–400 K.

The electrical resistivity  $\rho(T)$  for LaPtGe<sub>3</sub> decreases with decreasing temperature from 300 down to 1 K [Fig. 3(b)]. In this temperature range it fits nicely to the Bloch-Grüneisen (BG) formula [66,67] with  $n = 5$  [indicating  $\rho(T)$  is dominated by phonon-electron scattering processes],  $\rho_0 = 4.76(2) \mu\Omega \text{ cm}$ , phonon contribution coefficient  $A = 0.11(2) \mu\Omega \text{ cm}$ , and Debye temperature  $\Theta_R(0) = 230(3) \text{ K}$ .

The last value is in good agreement with  $\Theta_D(0) = 250 \text{ K}$  obtained from the specific heat (see below), which indicates

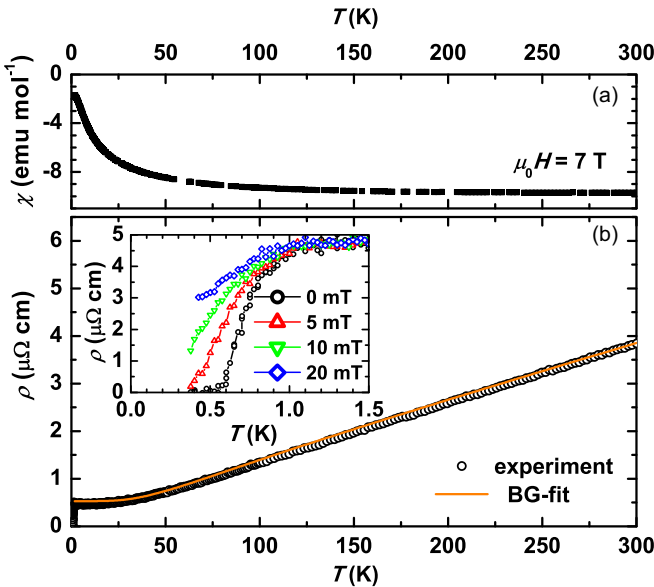


FIG. 3. (a) Magnetic susceptibility  $\chi(T)$  for LaPtGe<sub>3</sub>. (b) Electrical resistivity  $\rho(T)$  together with the BG fit. Inset: Evolution of  $\rho(T)$  near the SC transition in different magnetic fields.

that the low-temperature transport properties are mainly due to longitudinal phonons [68].

The electrical resistivity of LaPtGe<sub>3</sub> starts to drop below 1.2 K and becomes zero at  $T_c^0 = 0.57(1)$  K (Fig. 3, inset). Such a broad SC transition is most likely due to chemical inhomogeneities and crystallographic defects in the studied sample. As seen in the inset in Fig. 3, the width of the transition increases with increasing magnetic field, similar to what was reported for SrPtSi<sub>3</sub> [11], SrAuSi<sub>3</sub> [24], CaPtSi<sub>3</sub> [16], and AgMo<sub>6</sub>S<sub>8</sub> [69]. This makes the estimation of the critical magnetic field  $B_c$  challenging. Taking into account that the onset of superconductivity is still clearly visible for  $B = 20$  mT,  $B_c > 30$  mT is expected, which is much larger than the values obtained from the specific heat measurements (see discussion below). Since the difference between critical fields estimated from diverse methods exceeds the factor of 1.695 associated with  $B_{c3}$  surface superconductivity and thin limit physics [1], some other effects should be involved (e.g., anisotropy, enhanced superconductivity at the grain boundaries, etc. [16]).

The specific heat capacity of LaPtGe<sub>3</sub> in the  $c_p/T$  vs  $T^2$  presentation for various magnetic fields is plotted in the inset of Fig. 4. The data for  $B = 12$  mT are analyzed using the following equation, where the first term corresponds to the electronic specific heat  $c_{el}$  and the second one corresponds to the phononic contribution  $c_{ph}$ :

$$c_p(T) = \gamma_n T + \beta T^3. \quad (1)$$

The obtained values are  $\gamma_n = 3.50(1)$  mJ mol<sup>-1</sup> K<sup>-2</sup> and  $\beta = 0.62(2)$  mJ mol<sup>-1</sup> K<sup>-4</sup>, which indicates a Debye temperature  $\Theta_D = 250(3)$  K. After subtracting  $c_{ph}$ , the SC transition for zero field was analyzed by a graphical equal-area approximation (entropy conserving). This revealed  $T_c = 0.55(1)$  K [in agreement with  $T_c^0 = 0.57(1)$  K obtained from the electrical resistivity measurements] and the specific heat

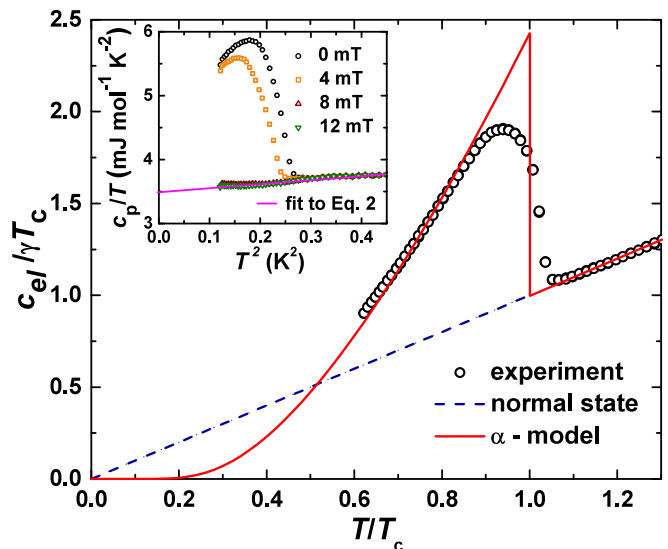


FIG. 4. Electronic specific heat for LaPtGe<sub>3</sub> and a comparison with the  $\alpha$  model [70]. The nonsuperconducting normal state  $c_{el} = \gamma_n T$  is given by a dashed line. Inset: Specific heat for LaPtGe<sub>3</sub> in various magnetic fields together with the fit to Eq. (1).

jump  $\Delta c_p/\gamma_n T_c = 1.26(4)$ , which is close to the prediction of the BCS theory (i.e., 1.43) for weak-coupled *s*-wave superconductors. Also, the electronic specific heat  $c_{el}$  of LaPtGe<sub>3</sub> below  $T_c$  fits nicely with the  $\alpha$  model for the BCS energy gap ratio  $\alpha_{BCS} \equiv \Delta(0)/k_B T_c \approx 1.764$  [70] (Fig. 4).

The specific heat anomaly of LaPtGe<sub>3</sub>, corresponding to the SC transition, is observed above 0.35 K only for  $B < 8$  mT (inset in Fig. 4). Using the two  $T_c$  values estimated from the jumps in  $c_p$  (Fig. 4, inset) the critical field  $B_c = 14$  mT is obtained. The calculation of the thermodynamic critical field for LaPtGe<sub>3</sub> [Eq. (2)] results in  $B_c = 13(2)$  mT, which indicates a type-I SC for the studied compound:

$$B_c^2 = 2(F_n - F_s) = -\gamma_n T_c^2 + 2 \int_0^{T_c} c_{el}(T) dT. \quad (2)$$

This finding is in line with the observed low  $T_c$  and  $B_c$  values, which are comparable with those reported for such type-I superconductors as simple metals [71], noncentrosymmetric TaSi<sub>2</sub> [72], and LaTSi<sub>3</sub> ( $T = \text{Rh, Ir, Pd}$ ) [21,26–28].

To obtain the microscopic superconducting parameters for LaPtGe<sub>3</sub> the free-electron model was applied, where the Sommerfeld coefficient is

$$\gamma = \frac{\pi^2 k_B^2 N_A m}{\hbar^2 (3\pi^2 n)^{2/3}}. \quad (3)$$

The calculated carrier density is  $n \simeq 4.6(2) \times 10^{27}$  m<sup>-3</sup>, the coherence length  $\xi_{BCS}(0) = 0.18\hbar v_F/k_B T_c = 1490(20)$  nm, and the penetration depth  $\lambda_{BCS}(0) = (m/\mu_0 n e^2)^{1/2} = 66(2)$  nm.

The electron-phonon coupling parameter is calculated in two ways: (i)  $\lambda = 0.37$  is obtained from the McMillan formula (with the repulsive screened Coulomb potential  $\mu^* = 0.1$ ):

$$\lambda = \frac{1.04 + \mu^* \ln(\Theta_D/1.45 T_c)}{(1 - 0.62\mu^*) \ln(\Theta_D/1.45 T_c) - 1.04}. \quad (4)$$

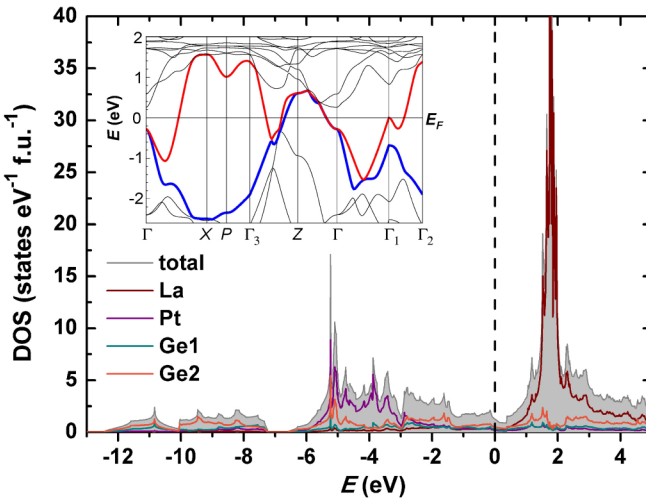


FIG. 5. Electronic density of states (DOS) for  $\text{LaPtGe}_3$ . Inset: The electronic band structure of  $\text{LaPtGe}_3$ . Only band 1 (red) and band 2 (blue) cross the Fermi level  $E_F$ .

(ii) The DFT calculations result in a DOS at the Fermi level  $N(E_F) = 1.27 \text{ states eV}^{-1} \text{f.u.}^{-1}$  (see below), which corresponds to the Sommerfeld coefficient  $\gamma_{\text{bare}} = 3 \text{ mJ mol}^{-1} \text{K}^{-2}$  and hence  $\lambda = (\gamma_n / \gamma_{\text{bare}}) - 1 = 0.17$ . Both obtained  $\lambda$  values for  $\text{LaPtGe}_3$  are well below 1, indicating a weak phonon-electron coupling, which is compatible with a type-I superconductivity.

The Fermi wave vector for the spherical Fermi surface is calculated as  $k_F = \sqrt[3]{3\pi^2 n} = 52(1) \text{ \AA}$ , and hence, the effective mass of the charge carriers

$$m^* = \frac{\gamma_n \hbar^2 k_F^2}{\pi^2 n k_B^2} = 2.2(1)m_e. \quad (5)$$

Taking the  $\rho_0$  value from the BG fit, we estimate the free mean time by applying the Drude model for the free-electron gas:  $\tau = m^*/\rho_0 n e^2 = 3.5(2) \times 10^{-13} \text{ s}$ , and the mean free path  $l = v_F \tau = (\hbar/m)(3\pi^2 n)^{1/3} \tau = 209(9) \text{ nm}$ , which is one order of magnitude smaller than the coherence length  $\xi_{\text{BCS}}(0)$ , thus indicating  $\text{LaPtGe}_3$  is in the dirty limit, similar to what was reported for the  $\text{LaIrSi}_3$  type-I superconductor [27]. For the dirty-limit superconductors the Ginzburg-Landau coherence length and the penetration depth are given as  $\xi_{\text{GL}}(0) = 8.57 \times 10^{-7} (\gamma \rho_0 T_c)^{-1/2} (1 - T/T_c)^{-1/2} = 8953(70) \text{ nm}$  and  $\lambda_{\text{GL}}(0) = 6.42 \times 10^{-3} (\rho_0/T_c)^{1/2} (1 - T/T_c)^{-1/2} = 189(2) \text{ nm}$ , respectively [73]. Hence, we calculate the Ginzburg-Landau parameter  $\kappa_{\text{GL}} = \lambda_{\text{GL}}(0)/\xi_{\text{GL}}(0) = 0.021(1) \leq 1/\sqrt{2}$ , again confirming  $\text{LaPtGe}_3$  is a type-I superconductor.

The electronic structure of  $\text{LaPtGe}_3$  is presented in Fig. 5. It features a low-energy separate region (extending from about  $-12.5$  to  $-7.2 \text{ eV}$ ) and a broad valence band ( $-6.6$  to  $0 \text{ eV}$ ) separated from each other by an energy gap of  $-0.6 \text{ eV}$ . The low-energy band is mainly due to the mixing of Ge 4s states, while the valence band is dominated by Ge 4p and Pt 5d electrons. The La 4f states form a broad maximum just above  $E_F$ . Also La 6s and 5d states lie at higher energies above  $E_F$ , which indicates a charge transfer from the positively charged La atoms towards the Pt-Ge anionic framework. The DOS at

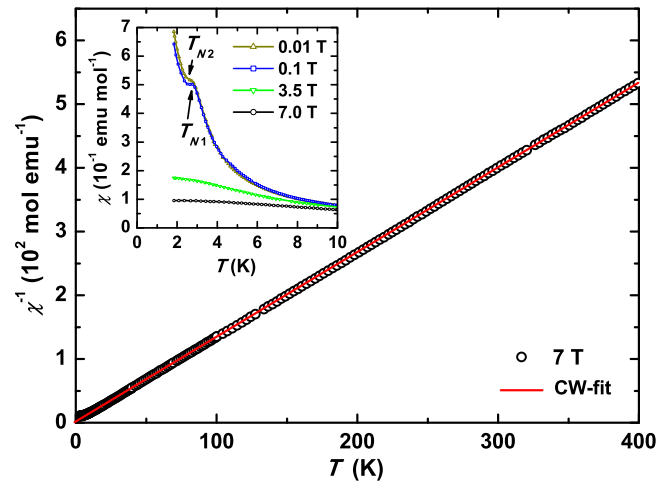


FIG. 6. Inverse magnetic susceptibility  $\chi^{-1}(T)$  for  $\text{CePtGe}_3$  together with the CW fit. The inset shows  $\chi(T)$  near the antiferromagnetic orderings in different magnetic fields.

$E_F$  is  $1.27 \text{ states eV}^{-1} \text{f.u.}^{-1}$  (mainly due to Ge 4p states), which indicates  $\text{LaPtGe}_3$  is a simple metallic system. Similar features of the electronic structure were reported for such superconductors as the filled skutterudite  $\text{LaPt}_4\text{Ge}_{12}$  [74] and  $\text{Y}_3\text{Pt}_4\text{Ge}_{13}$  [45].

The electronic band structure of  $\text{LaPtGe}_3$  near the Fermi level is given in the inset of Fig. 5. It is similar to those reported for isostructural  $\text{SrAuSi}_3$  [24], where only two bands cross  $E_F$ .

### C. $\text{CePtGe}_3$

The temperature dependence of the inverse magnetic susceptibility  $\chi^{-1}(T)$  of the  $\text{CePtGe}_3$  phase is depicted in Fig. 6. In the temperature range  $50$ – $300 \text{ K}$  the susceptibility fits the Curie-Weiss (CW) law with an effective magnetic moment  $\mu_{\text{eff}} = 2.46 \mu_B$  (close to the free-ion value  $2.54 \mu_B$  for a  $\text{Ce}^{3+}$  ion) and small negative Weiss temperature  $\theta_{\text{CW}} = -1.8 \text{ K}$ . These results confirm that the properties of  $\text{CePtGe}_3$  are not affected by the minor impurity  $\text{Ce}_2\text{Pt}_3\text{Ge}_5$  phase, where  $\theta_{\text{CW}} = -39.2 \text{ K}$  is reported [62].  $\text{CePtGe}_3$  shows two magnetic ordering transitions at  $T_{N1} \approx 3.1 \text{ K}$  and  $T_{N2} \approx 2.5 \text{ K}$  (inset in Fig. 6), as does the isostructural  $\text{Ce}\{\text{Rh}, \text{Ir}\}\text{Ge}_3$  [41,42] and structurally related  $\text{CeAu}_2\text{Ge}_2$  [75]. Since both of them can be suppressed by fields  $\mu_0 H > 3.5 \text{ T}$  (to  $T < 1.8 \text{ K}$ ), they indicate bulk antiferromagnetic (AF) ordering for  $\text{CePtGe}_3$ . The  $T_N$  observed here are well below  $T_N = 4 \text{ K}$ , which was reported for  $\text{Ce}_2\text{Pt}_3\text{Ge}_5$  [63] (the minor impurity phase identified in our sample).

The electrical resistivity of  $\text{CePtGe}_3$  is one order of magnitude larger than that of  $\text{LaPtGe}_3$  [Figs. 3(b) and 7]. It decreases linearly down to a temperature of  $\sim 120 \text{ K}$ ; then the slope increases, and the resistivity falls to  $\approx 5 \mu\Omega \text{ cm}$  at  $7 \text{ K}$ . Such a broad curvature can originate from the combination of such effects as the crystal electric field (CEF) and weak Kondo interaction. The single-ion Kondo model [76] suggests the position of the curvature maximum (i.e.,  $\sim 120 \text{ K}$ ) to give a rough estimate of the total CEF splitting energy. This value is in good agreement with the overall splitting of  $137 \text{ K}$

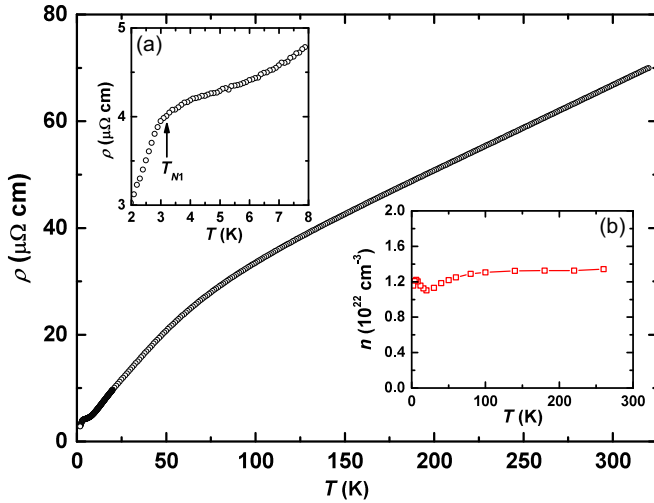


FIG. 7. Electrical resistivity  $\rho(T)$  for  $\text{CePtGe}_3$  ( $\mu_0 H = 0$  T). (a)  $\rho(T)$  near the antiferromagnetic ordering. (b) Temperature dependence of the charge carrier concentration  $n$  for  $\text{CePtGe}_3$ .

obtained from the specific heat data (see below). The  $\rho(T)$  of  $\text{CePtGe}_3$  reveals features similar to those reported for  $\text{CeIr}_2\text{B}_2$  [77]. A further drastic decrease of  $\rho(T)$  occurs at  $\approx 3.2$  K [Fig. 7(a)], which is in good agreement with  $T_{N1}$ , the AF ordering temperature in  $\text{CePtGe}_3$ . As determined from Hall-effect measurements, the charge carrier (holes) concentration  $h(T)$  [Fig. 7(b)] is almost temperature independent ( $1.10\text{--}1.34 \times 10^{22} \text{ cm}^{-3}$ ). These values are in fair agreement with the carrier concentration calculated for  $\text{LaPtGe}_3$  and are within the range observed for several other metallic ternary transition-metal compounds.

The specific heat  $c_p(T)$  for  $\text{CePtGe}_3$  (Fig. 8) reveals three anomalies centered at  $T_{N1} \approx 3.7$  K,  $T_{N2} \approx 2.7$  K, and  $T^* \approx 1.5$  K. The first two agree well with magnetic ordering observed in  $\chi(T)$  measurements, while the nature of the anomaly at  $T^*$  is less clear. A similar shoulder in the specific

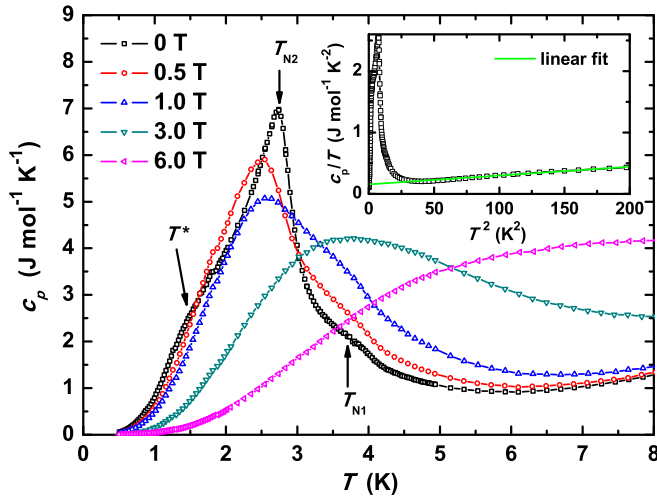


FIG. 8. Specific heat versus temperature for  $\text{CePtGe}_3$  in different magnetic fields. The inset displays  $c_p/T$  versus  $T^2$  together with a linear fit for  $T$  above the observed anomalies.

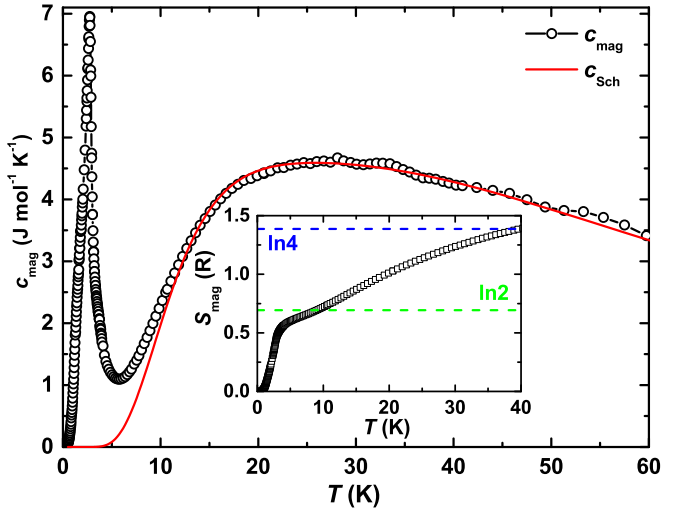


FIG. 9. Magnetic specific heat  $c_{\text{mag}}$  versus temperature for  $\text{CePtGe}_3$  together with the three-level Schottky anomaly fit based on the CEF model (see text). The inset shows the integrated entropy with two horizontal dashed lines corresponding to  $R\text{In}2$  and  $R\text{In}4$  values, respectively.

heat just below a  $\lambda$  anomaly corresponding to an antiferromagnetic transition is reported for isostructural  $\text{EuPtGe}_3$  [43]. There, the shoulder is explained by a combination of contributions of a Schottky anomaly and magnons. However, such a scenario can be excluded in the case of the doublet ground state of  $\text{Ce}^{3+}$  ions. The linear extrapolation of  $c_p/T$  versus  $T^2$  dependence (inset in Fig. 8) results in an estimation of the Sommerfeld coefficient  $\gamma_0 \approx 155(5) \text{ mJ mol}^{-1} \text{ K}^{-2}$ . This moderately enhanced value is comparable to those reported for the structurally related  $\text{CeNi}_2\text{As}_2$  [78] and  $\text{CeAu}_2\text{Ge}_2$  [75] compounds and indicates correlation effects originating from the Ce 4f electrons. In a field of 0.5 T the anomalies at  $T_{N1}$  and  $T_{N2}$  shift towards lower temperatures (Fig. 8), which is a fingerprint of the antiferromagnetic nature of both orderings. A further increase of the magnetic field leads to the broadening of the anomalies. The Schottky-type dependence observed in the specific heat of  $\text{CePtGe}_3$  for  $\mu_0 H > 3$  T indicates the splitting of the ground-state doublet by the Zeeman effect.

The magnetic specific heat  $c_{\text{mag}}$  for  $\text{CePtGe}_3$  is obtained by subtracting  $c_{\text{ph}}$  of the phonon-reference compound  $\text{LaPtGe}_3$ . A broad maximum in  $c_{\text{mag}}$  centered at  $\sim 30$  K (Fig. 9) is due to a Schottky anomaly arising from the  $\text{Ce}^{3+}$  ground-state multiplet  $J = 5/2$  splitting into three doublets. Thus, applying the formula for the Schottky contribution for a three-level system, we obtained the energy splitting from the ground state  $\Delta_1 = 46.0(2)$  K and  $\Delta_2 = 136.7(8)$  K. The magnetic entropy  $S_{\text{mag}}$  for  $\text{CePtGe}_3$  is plotted in the inset in Fig. 9. It reaches a value of  $R\text{In}4$  at  $\sim 41$  K, which further supports the energy splitting of 46 K between the ground state and the first excited state. The magnetic entropy  $S_{\text{mag}} \sim 0.8R\text{In}2$  at  $T_{N1} = 3.7$  K is slightly lower than the expected critical value and agrees well with the prediction of the Ising model for fcc lattices (e.g.,  $0.85R\text{In}2$ ) [79]. This finding together with an enhanced Sommerfeld coefficient  $\gamma$  may suggest a very weak Kondo effect in the studied compound. Using the mean-field theoretical universal plot of the jump in specific heat  $\Delta c_{\text{mag}}$

vs  $T_K/T_m$  proposed in [80], we found  $T_K/T_m \approx 0.82$  for  $\Delta c_{\text{mag}} = 6.1 \text{ J mol}^{-1} \text{ K}^{-1}$ , and hence,  $T_K \approx 2.3 \text{ K}$  at  $T_{N2} = 2.75 \text{ K}$ . Thus, we conclude that in CePtGe<sub>3</sub> the magnetic Ruderman-Kittel-Kasuya-Yosida (RKKY)-type interaction is strongly dominating, resulting in the magnetically ordered states at low temperatures.

#### IV. CONCLUSIONS

New LaPtGe<sub>3</sub> and CePtGe<sub>3</sub> germanides were synthesized by the arc-melting method and by applying high-pressure, high-temperature synthesis, respectively. Rietveld crystal structure refinement performed on the high-resolution x-ray diffraction powder patterns confirmed both of the compounds crystallize with the noncentrosymmetric BaNiSn<sub>3</sub> type (space group *I4mm*).

The measurements of the magnetic susceptibility reveal LaPtGe<sub>3</sub> is a diamagnet, while the temperature dependence of the electrical resistivity in agreement with the theoretical DFT calculations indicates LaPtGe<sub>3</sub> is a simple metallic system. At  $T_c = 0.55 \text{ K}$  LaPtGe<sub>3</sub> becomes superconducting with a critical field  $B_c \approx 14 \text{ mT}$ , which together with the Ginzburg-Landau parameter  $\kappa_{\text{GL}} = \lambda_{\text{GL}}(0)/\xi_{\text{GL}}(0) = 0.021(1) < 1/\sqrt{2}$  indicates that LaPtGe<sub>3</sub> is a type-I superconductor with weak electron-phonon coupling and *s*-wave BCS-like superconductivity.

Above 50 K CePtGe<sub>3</sub> is a paramagnet with an effective magnetic moment  $\mu_{\text{eff}} = 2.46 \mu_B$ , which is close to that of

the free Ce<sup>3+</sup> ion. Measurements of magnetic susceptibility and specific heat reveal two antiferromagnetic transitions at  $T_{N1} \approx 3.7 \text{ K}$  and  $T_{N2} \approx 2.7 \text{ K}$  for CePtGe<sub>3</sub>. The origin of the anomaly at  $T^* \approx 1.5 \text{ K}$  observed in the specific heat is unclear. Obviously, to clarify the magnetic structure of CePtGe<sub>3</sub> a study of a single-crystalline material would be required. The magnetic specific heat of CePtGe<sub>3</sub> shows a clear Schottky anomaly corresponding to the Ce<sup>3+</sup> ground-state multiplet  $J = 5/2$  splitting into three doublets with the splitting energies from the ground state  $\Delta_1 = 46.0(2) \text{ K}$  and  $\Delta_2 = 136.7(8) \text{ K}$ . The slightly lower magnetic entropy  $S_{\text{mag}} \sim 0.8R \ln 2$  at  $T_{N1} = 3.7 \text{ K}$  together with the moderately enhanced Sommerfeld coefficient  $\gamma_0 \approx 155(5) \text{ mJ mol}^{-1} \text{ K}^{-2}$  suggests only weak Kondo interactions and thus dominating RKKY interactions, resulting in an antiferromagnetically ordered ground state in CePtGe<sub>3</sub>. No superconductivity was detected for  $T > 0.35 \text{ K}$ .

#### ACKNOWLEDGMENTS

M.F. is grateful to DFG (Deutsche Forschungsgemeinschaft) for financial support (Grant No. GU1632/4-1). The authors are indebted to H. Borrmann for performing XRD measurements and S. Leipe for assistance during the high-pressure syntheses. The authors are also grateful to E. Svanidze for fruitful discussions. We also thank Y. Grin for his continuous support and interest in this work.

- 
- [1] *Non-centrosymmetric Superconductors*, edited by E. Bauer and M. Sigrist (Springer, Berlin, 2012).
  - [2] A. D. Hillier, J. Quintanilla, and R. Cywinski, *Phys. Rev. Lett.* **102**, 117007 (2009).
  - [3] J. Quintanilla, A. D. Hillier, J. F. Annett, and R. Cywinski, *Phys. Rev. B* **82**, 174511 (2010).
  - [4] E. Bauer, G. Rogl, X.-Q. Chen, R. T. Khan, H. Michor, G. Hilscher, E. Royanian, K. Kumagai, D. Z. Li, Y. Y. Li *et al.*, *Phys. Rev. B* **82**, 064511 (2010).
  - [5] A. B. Karki, Y. M. Xiong, I. Vekhter, D. Browne, P. W. Adams, D. P. Young, K. R. Thomas, J. Y. Chan, H. Kim, and R. Prozorov, *Phys. Rev. B* **82**, 064512 (2010).
  - [6] I. Bonalde, H. Kim, R. Prozorov, C. Rojas, P. Rogl, and E. Bauer, *Phys. Rev. B* **84**, 134506 (2011).
  - [7] E. Bauer, C. Sekine, U. Sai, P. Rogl, P. K. Biswas, and A. Amato, *Phys. Rev. B* **90**, 054522 (2014).
  - [8] H. Q. Yuan, D. F. Agterberg, N. Hayashi, P. Badica, D. Vandervelde, K. Togano, M. Sigrist, and M. B. Salamon, *Phys. Rev. Lett.* **97**, 017006 (2006).
  - [9] M. Nishiyama, Y. Inada, and G.-Q. Zheng, *Phys. Rev. Lett.* **98**, 047002 (2007).
  - [10] W. Dörrscheidt and H. Schäfer, *J. Less-Common Met.* **58**, 209 (1978).
  - [11] F. Kneidinger, L. Salamakha, E. Bauer, I. Zeiringer, P. Rogl, C. Blaas-Schenner, D. Reith, and R. Podloucky, *Phys. Rev. B* **90**, 024504 (2014).
  - [12] G. Eguchi, D. Peets, M. Kriener, S. Maki, E. Nishibori, H. Sawa, and Y. Maeno, *Physica C (Amsterdam, Neth.)* **470**, S762 (2010).
  - [13] R. P. Singh, A. D. Hillier, D. Chowdhury, J. A. T. Barker, D. M. Paul, M. R. Lees, and G. Balakrishnan, *Phys. Rev. B* **90**, 104504 (2014).
  - [14] B. A. Frandsen, S. C. Cheung, T. Goko, L. Liu, T. Medina, T. S. J. Munsie, G. M. Luke, P. J. Baker, M. P. Jimenez S., G. Eguchi *et al.*, *Phys. Rev. B* **91**, 014511 (2015).
  - [15] H. Uzunok, E. Ipsara, H. Tütüncü, G. Srivastava, and A. Başoğlu, *J. Alloys Compd.* **681**, 205 (2016).
  - [16] G. Eguchi, D. C. Peets, M. Kriener, Y. Maeno, E. Nishibori, Y. Kumazawa, K. Banno, S. Maki, and H. Sawa, *Phys. Rev. B* **83**, 024512 (2011).
  - [17] V. V. Bannikov, I. R. Shein, and A. L. Ivanovskii, *JETP Lett.* **92**, 343 (2010).
  - [18] E. Bauer, R. T. Khan, H. Michor, E. Royanian, A. Grytsiv, N. Melnychenko-Koblyuk, P. Rogl, D. Reith, R. Podloucky, E.-W. Scheidt *et al.*, *Phys. Rev. B* **80**, 064504 (2009).
  - [19] R. Ribeiro-Palau, R. Caraballo, P. Rogl, E. Bauer, and I. Bonalde, *J. Phys.: Condens. Matter* **26**, 235701 (2014).
  - [20] K. Miliyanchuk, F. Kneidinger, C. Blaas-Schenner, D. Reith, R. Podloucky, P. Rogl, T. Khan, L. Salamakha, G. Hilscher, H. Michor *et al.*, *J. Phys.: Conf. Series* **273**, 012078 (2011).
  - [21] M. Smidman, A. D. Hillier, D. T. Adroja, M. R. Lees, V. K. Anand, R. P. Singh, R. I. Smith, D. M. Paul, and G. Balakrishnan, *Phys. Rev. B* **89**, 094509 (2014).
  - [22] H. Uzunok, H. Tütüncü, G. Srivastava, and A. Başoğlu, *Intermetallics* **86**, 1 (2017).
  - [23] M. Isobe, H. Yoshida, K. Kimoto, M. Arai, and E. Takayama-Muromachi, *Chem. Mater.* **26**, 2155 (2014).

- [24] M. Isobe, M. Arai, and N. Shirakawa, *Phys. Rev. B* **93**, 054519 (2016).
- [25] N. Barbero, P. K. Biswas, M. Isobe, A. Amato, E. Morenzoni, A. D. Hillier, H.-R. Ott, J. Mesot, and T. Shiroka, *Phys. Rev. B* **97**, 024501 (2018).
- [26] V. K. Anand, A. D. Hillier, D. T. Adroja, A. M. Strydom, H. Michor, K. A. McEwen, and B. D. Rainford, *Phys. Rev. B* **83**, 064522 (2011).
- [27] V. K. Anand, D. Britz, A. Bhattacharyya, D. T. Adroja, A. D. Hillier, A. M. Strydom, W. Kockelmann, B. D. Rainford, and K. A. McEwen, *Phys. Rev. B* **90**, 014513 (2014).
- [28] D. Kawakatsu, A. Sumiyama, J. Gouchi, A. Yamaguchi, G. Motoyama, Y. Hirose, R. Settai, and Y. Ōnuki, *J. Phys. Soc. Jpn.* **85**, 025002 (2016).
- [29] R. Troć, R. Wawryk, and A. Gribanov, *J. Alloys Compd.* **581**, 659 (2013).
- [30] T. Kawai, H. Muranaka, T. Endo, N. Duc Dung, Y. Doi, S. Ikeda, T. Matsuda, Y. Haga, H. Harima, R. Settai *et al.*, *J. Phys. Soc. Jpn.* **77**, 064717 (2008).
- [31] E. Bauer, G. Hilscher, H. Michor, C. Paul, E. W. Scheidt, A. Gribanov, Y. Seropegin, H. Noël, M. Sigrist, and P. Rogl, *Phys. Rev. Lett.* **92**, 027003 (2004).
- [32] M. Nicklas, F. Steglich, J. Knolle, I. Eremin, R. Lackner, and E. Bauer, *Phys. Rev. B* **81**, 180511 (2010).
- [33] N. Kimura, K. Ito, K. Saitoh, Y. Umeda, H. Aoki, and T. Terashima, *Phys. Rev. Lett.* **95**, 247004 (2005).
- [34] F. Tomioka, M. Hedo, I. Umehara, T. Ono, Y. Uwatoko, N. Kimura, and S. Takayanagi, *J. Magn. Magn. Mater.* **310**, 340 (2007).
- [35] N. Kimura, K. Ito, H. Aoki, S. Uji, and T. Terashima, *Phys. Rev. Lett.* **98**, 197001 (2007).
- [36] N. Tateiwa, Y. Haga, T. D. Matsuda, S. Ikeda, E. Yamamoto, Y. Okuda, Y. Miyauchi, R. Settai, and Y. Ōnuki, *J. Phys.: Conf. Ser.* **121**, 052001 (2008).
- [37] H. Mukuda, T. Fujii, T. Ohara, A. Harada, M. Yashima, Y. Kitaoka, Y. Okuda, R. Settai, and Y. Ōnuki, *Phys. Rev. Lett.* **100**, 107003 (2008).
- [38] Y. Ōnuki, H. Shishido, Y. Okuda, Y. Miyauchi, R. Settai, T. Takeuchi, T. Matsuda, N. Tateiwa, Y. Haga, and H. Harima, *Physica B (Amsterdam, Neth.)* **403**, 963 (2008).
- [39] R. Settai, I. Sugitani, Y. Okuda, A. Thamizhavel, M. Nakashima, Y. Ōnuki, and H. Harima, *J. Magn. Magn. Mater.* **310**, 844 (2007).
- [40] R. Settai, Y. Okuda, I. Sugitani, Y. Ōnuki, T. D. Matsuda, Y. Haga, and H. Harima, *Int. J. Mod. Phys. B* **21**, 3238 (2007).
- [41] H. Wang, J. Guo, E. D. Bauer, V. A. Sidorov, H. Zhao, J. Zhang, Y. Zhou, Z. Wang, S. Cai, K. Yang *et al.*, *Phys. Rev. B* **97**, 064514 (2018).
- [42] F. Honda, I. Bonalde, K. Shimizu, S. Yoshiuchi, Y. Hirose, T. Nakamura, R. Settai, and Y. Ōnuki, *Phys. Rev. B* **81**, 140507 (2010).
- [43] N. Kumar, P. Das, R. Kulkarni, T. Thamizhavel, S. K. Dhar, and P. Bonville, *J. Phys.: Condens. Matter* **24**, 036005 (2012).
- [44] R. Gumeniuk, L. Akselrud, K. O. Kvashnina, W. Schnelle, A. A. Tsirlin, C. Curfs, H. Rosner, M. Schöneich, U. Burkhardt, U. Schwarz *et al.*, *Dalton Trans.* **41**, 6299 (2012).
- [45] R. Gumeniuk, M. Nicklas, L. Akselrud, W. Schnelle, U. Schwarz, A. A. Tsirlin, A. Leithe-Jasper, and Y. Grin, *Phys. Rev. B* **87**, 224502 (2013).
- [46] R. Gumeniuk, M. Schöneich, K. O. Kvashnina, L. Akselrud, A. A. Tsirlin, M. Nicklas, W. Schnelle, O. Janson, Q. Zheng, C. Curfs *et al.*, *Dalton Trans.* **44**, 5638 (2015).
- [47] J. Remeika, G. Espinosa, A. Cooper, H. Barz, J. Rowell, D. McWhan, J. Vandenberg, D. Moncton, Z. Fisk, L. Woolf *et al.*, *Solid State Commun.* **34**, 923 (1980).
- [48] D. Walker, M. A. Carpenter, and C. M. Hitch, *Am. Mineral.* **75**, 1020 (1990).
- [49] E. F. Eikenberry, C. Brönnimann, G. Hülsen, H. Toyokawa, R. Horisberger, B. Schmitt, C. Schulze-Briese, and T. Tomizaki, *Nucl. Instrum. Methods Phys. Res., Sect. A* **501**, 260 (2003).
- [50] V. Dyadkin, P. Pattison, V. Dmitriev, and D. Chernyshov, *J. Synchrotron Radiat.* **23**, 825 (2016).
- [51] J. Kieffer and D. Karkoulis, *J. Phys.: Conf. Ser.* **425**, 202012 (2013).
- [52] STOE Powder Software, WINXPOW, version 2, STOE and Cie, Darmstadt, 2001.
- [53] L. Akselrud and Y. Grin, *J. Appl. Crystallogr.* **47**, 803 (2014).
- [54] K. Koepernik and H. Eschrig, *Phys. Rev. B* **59**, 1743 (1999).
- [55] J. P. Perdew and Y. Wang, *Phys. Rev. B* **45**, 13244 (1992).
- [56] R. D. Shannon, *Acta Crystallogr., Sect. A* **32**, 751 (1976).
- [57] Z. Ban and M. Sikirica, *Acta Crystallogr.* **18**, 594 (1965).
- [58] D. Rossi, R. Marazza, and R. Ferro, *J. Less-Comm. Met.* **66**, P17 (1979).
- [59] M. François, G. Venturini, E. McRae, B. Malaman, and B. Roques, *J. Less-Common Met.* **128**, 249 (1987).
- [60] A. Gribanov, O. Sologub, P. Salamakha, O. Bodak, Y. Seropegin, and V. Pecharsky, *J. Alloys Compd.* **179**, L7 (1992).
- [61] A. Dommann, F. Hulliger, H. Ott, and V. Gramlich, *J. Less-Common Metals* **110**, 331 (1985).
- [62] R. Gumeniuk, K. Kvashnina, W. Schnelle, M. Nicklas, H. Borrmann, H. Rosner, Y. Skourski, A. A. Tsirlin, A. Leithe-Jasper, and Y. Grin, *J. Phys.: Condens. Matter* **23**, 465601 (2011).
- [63] A. T. B. Rosch, Ph.D. thesis, TU Braunschweig, 2004.
- [64] J. Emsley, *The Elements* (Clarendon Press, Oxford, 1998).
- [65] D. Kußmann, R. Pöttgen, U. C. Rodewald, C. Rosenhahn, B. D. Mosel, G. Kotzyba, and B. Künnen, *Z. Naturforsch. B* **54**, 1155 (1999).
- [66] E. Grüneisen, *Ann. Phys. (Berlin, Ger.)* **408**, 530 (1933).
- [67] E. Grüneisen and H. Reddemann, *Ann. Phys. (Berlin, Ger.)* **412**, 843 (1934).
- [68] E. S. R. Gopal, *Specific Heat at Low Temperatures* (Plenum Press, London, 1966).
- [69] M. Feig, M. Bobnar, I. Veremchuk, C. Hennig, U. Burkhardt, R. Starke, B. Kundys, A. Leithe-Jasper, and R. Gumeniuk, *J. Phys.: Condens. Matter* **29**, 495603 (2017).
- [70] D. Johnston, *Supercond. Sci. Technol.* **26**, 115011 (2013).
- [71] N. Ashcroft and N. Mermin, *Solid State Physics* (Harcourt College Publishers, Fort Worth TX, Orlando FL, 1976).
- [72] U. Gottlieb, J. C. Lasjaunias, J. L. Tholence, O. Laborde, O. Thomas, and R. Madar, *Phys. Rev. B* **45**, 4803 (1992).
- [73] T. P. Orlando, E. J. McNiff, S. Foner, and M. R. Beasley, *Phys. Rev. B* **19**, 4545 (1979).
- [74] R. Gumeniuk, W. Schnelle, H. Rosner, M. Nicklas, A. Leithe-Jasper, and Y. Grin, *Phys. Rev. Lett.* **100**, 017002 (2008).

- [75] C. Huang, V. Fritsch, W. Kittler, and H. Löhneysen, *Phys. Rev. B* **86**, 214401 (2012).
- [76] B. Cornut and B. Coqblin, *Phys. Rev. B* **5**, 4541 (1972).
- [77] A. Prasad, V. K. Anand, U. B. Paramanik, Z. Hossain, R. Sarkar, N. Oeschler, M. Baenitz, and C. Geibel, *Phys. Rev. B* **86**, 014414 (2012).
- [78] Y. Luo, J. Bao, C. Shen, J. Han, X. Yang, C. Lv, Y. Li, W. Jiao, B. Si, C. Feng *et al.*, *Phys. Rev. B* **86**, 245130 (2012).
- [79] L. J. D. Jongh and A. R. Miedema, *Adv. Phys.* **50**, 947 (2001).
- [80] M. Besnus, A. Braghta, N. Hamdaoui, and A. Meyer, *J. Magn. Magn. Mater.* **104**, 1385 (1992).